

Multiferroicity and spiral magnetism in FeVO_4 with quenched Fe orbital moments

A. Daoud-Aladine,¹ B. Kundys,² C. Martin,² P.G. Radaelli,^{1,3} P.J. Brown,⁴ C. Simon,² and L. C. Chapon¹

¹*ISIS facility, Rutherford Appleton Laboratory-CCLRC,
Chilton, Didcot, Oxfordshire, OX11 0QX, United Kingdom.*

²*Laboratoire CRISMAT-UMR, 6508 ENSI CAEN, 6, Marechal Juin, 14050 Caen, France*

³*Dept. of Physics and Astronomy, University College London,
Gower Street, London WC1E 6BT, United Kingdom*

⁴*Institut Laue Langevin, 6 rue Jules Horowitz, BP 156, 38042 Grenoble Cedex 9, France*

(Dated: November 2, 2018)

FeVO_4 has been studied by heat capacity, magnetic susceptibility, electric polarization and single crystal neutron diffraction experiments. The triclinic crystal structure is made of S -shaped clusters of six Fe^{3+} ions, linked by VO_4^{3-} groups. Two long-range magnetic ordering transitions occur at $T_{N1}=22\text{K}$ and $T_{N2}=15\text{K}$. Both magnetic structures are incommensurate. That stable below T_{N1} is collinear with amplitude modulated moments whereas below T_{N2} the arrangement is non-collinear with a helicoidal modulation. Below T_{N2} , FeVO_4 becomes weakly ferroelectric coincidentally with the loss of the collinearity of the magnetic structure. We conclude that FeVO_4 provides another example of frustrated spiral magnet similar to the classical TbMnO_3 compound. However, FeVO_4 has quenched orbital moments and a particular structure clarifying the respective role of anisotropy and magnetic frustration in this type of multiferroic materials.

PACS numbers: 25.40.Dn, 75.25.+z, 77.80.-e

There has been a recent surge of interest in a novel class of multiferroic materials[1], in which ferroelectricity arises below a magnetic phase transition and as a direct consequence of complex magnetic ordering in systems with strong magneto-electric interactions[2]. This phenomenon, which requires lowering of the magneto-crystalline symmetry to a polar group, can only appear in complex magnetic structures, typically stabilized by magnetic frustration or strong exchange competition, as in $\text{Ni}_3\text{V}_2\text{O}_8$ [3] and TbMnO_3 [4]. By contrast, these "novel" or "type II" multiferroics are simple binary [5] or ternary oxides — a desirable feature for prospective applications.

In addition to fulfilling strict magneto-structural symmetry requirements, type-II multiferroics must possess a microscopic mechanism to generate electric dipole moments. A variety of such mechanisms have been proposed [6]: magneto-striction is the only allowed mechanism for acentric collinear structures, and is active in the Ising system $\text{Ca}_3(\text{Co,Mn})_2\text{O}_6$ [7] and, most likely, in the commensurate phase of YMn_2O_5 [8]. Most other "type-II" multiferroics are cycloidal magnets, where non-collinear spins are key ingredients in the context of the so-called spin-current model [9, 10]. For this, a crucial role is played by relativistic spin-orbit interaction, which can take place at the ligand ionic site, as for pure e_g systems, within the transition-metal t_{2g} orbitals or between t_{2g} and e_g orbitals [6]. A particularly interesting case of the latter is provided by high-spin d^5 systems ($S=5/2$) where $L=0$ in the free ion and the orbital angular momentum is supposedly absent. As for the acentric magnetic structure itself, this typically comes about when a connected network of superexchange (SE) interactions is destabilized by the presence of either strong next-nearest neighbor in-

teractions or geometrical frustration [1, 11].

In this letter, we describe a new multiferroic compound — FeVO_4 — in which the magnetic ion is orbitally quenched Fe^{3+} (d^5 , $L=0$, $S=5/2$). The magnetic and dielectric phase diagram of FeVO_4 , as determined from magnetization, specific heat and neutron diffraction measurements, is that of a typical cycloidal magnet: ferroelectricity appears below $T_{N2}=15\text{K}$, coinciding with the appearance of a non-collinear incommensurate magnetic structure (phase II), whereas a second collinear incommensurate magnetic phase (I), stable between $T_{N1}=22\text{K}$ and T_{N2} , is not ferroelectric. Uniquely, FeVO_4 does not contain connected magnetic direct exchange or SE paths, and the magnetic modulation is primarily determined by a network of super-super-exchange (SSE) interactions. These pathways form loops connecting an odd number of Fe^{3+} , suggesting that frustration plays a key role in promoting non-collinearity and ferroelectricity.

Polycrystalline samples and single crystals were prepared following the procedures described in Refs 12 and 13. Electric measurements and specific heat and magnetic susceptibility measurements were carried out on dense pellets of polycrystalline FeVO_4 using a PPMS Quantum Design cryostat. The electrical polarization was derived from integration of the pyroelectric current measured with a Keithley 6517 electrometer. Magnetization measurements on single crystals were made with a vertical-field SQUID magnetometer using a horizontal axis sample-rotator. Single crystal neutron nuclear and magnetic Bragg peak intensities were collected and at $T=2\text{K}$ and $T=18\text{K}$ on the four-circle diffractometer D15 ($\lambda = 1.174\text{\AA}$) at the Institut Laue-Langevin (ILL), France. All the nuclear and magnetic structure refinements were carried out with the program FullProf[14].

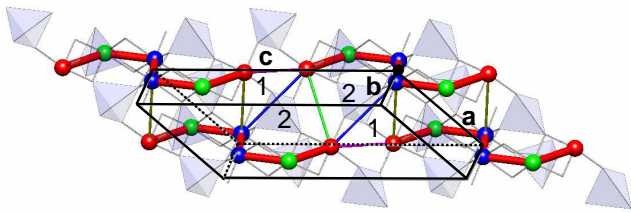


FIG. 1: (Color) (a) Crystal structure and magnetic exchange frustration in FeVO_4 . The basic magnetic unit are S -shaped clusters made of 6 Fe^{3+} atoms (red, blue, and green large balls) well spaced by V^{5+}O_4 tetrahedra (blue). The Fe-O bonds are drawn as thin grey lines (O atoms are not shown for clarity). The thick red lines represent intra-cluster interactions, with contributions from direct Fe-Fe exchange and Fe-O-Fe super-exchange. Iron atoms belonging to different clusters are coupled by Fe-O-O-Fe SSE paths mediated by the edges of the VO_4^{3-} tetrahedra giving rise to effective inter-cluster Fe-Fe interactions (thin colored lines)

The crystal structure of FeVO_4 is shown in Fig. 1. To facilitate the description of the magnetic structures (see below) we have redefined the triclinic basis vector \mathbf{c} so that $\mathbf{c} = -2\mathbf{a}' - \mathbf{c}'$, where \mathbf{a}' and \mathbf{c}' are the basis vectors used in Ref.13. The important crystallographic features for the description of the magnetic properties are easily identified. The Fe^{3+} ions, all in the high-spin state $S=5/2$ (see below), are arranged in clusters, separated by $(\text{VO}_4)^{3-}$ groups, containing non-magnetic V^{5+} ions. Each cluster of 6 Fe^{3+} ions consists of two identical Fe_3O_{13} monomers, related by a center of inversion. With our convention, the \mathbf{c} -axis runs along the line connecting adjacent clusters through their centers and open ends. In Fig1, we have also represented the two main types of magnetic interactions: intra-cluster direct-exchange and SE interactions (thick lines), which are antiferromagnetic (AF), and inter-cluster SSE interactions (thin lines). There is clearly the potential for magnetic frustration, since Fig.1 reveals that the effective inter-cluster and intra-cluster Fe-Fe linkages form loops (label 1 and 2), which contain an odd number of Fe sites, within which collinear AF arrangements cannot be fully satisfied.

The magnetic frustration and competition between SE and SSE interactions give rise to a complex low temperature phase diagram, reminiscent of that of other cycloidal magnets. Above 100 K the magnetic susceptibility follows a Curie-Weiss law (not shown). The effective paramagnetic moment $\mu_{eff} = 6.103(4)\mu_B$ is near the value expected for Fe^{3+} ions in the high-spin $S=5/2$ state ($\mu_{eff}^{th} = 5.91\mu_B$). The Weiss temperature $\theta_{CW} = -124.9(4)\text{K}$ confirms the presence of strong AF interactions. The low temperature data clearly indicate magnetic transitions at $T_{N1}=22\text{K}$ and $T_{N2}=15\text{K}$, consistent with a frustration index of $|\theta_{CW}|/T_{N1} \sim 6$. The specific heat, (Fig. 2 a) also shows two lambda-type anoma-

lies at these critical temperatures. The magnetic contribution to the specific heat was determined by subtracting the lattice contribution, indicated by the dashed line in Fig. 2 a), which was estimated by fitting the data at high temperature to the Debye function (Debye temperature of $385(5)\text{K}$). The magnetic entropy integrated between 2K and 50K is $S_M = 13.98 \text{ J.K}^{-1}.\text{mol}^{-1}$, approaching the classical value of $R \log(2S + 1) = 14.89 \text{ J.K}^{-1}.\text{mol}^{-1}$ for $S=5/2$. A large fraction of the total magnetic entropy ($\sim 30\%$) is only recovered far above T_{N1} , indicative of short-range AF ordering above T_{N1} [15].

To obtain further insight into the nature of the magnetic ordering taking place at T_{N1} and T_{N2} , magnetic measurements were made on the needle-shaped single crystals. The crystal orientation was set at 300K before cooling the crystal in a 3-T field and recording magnetization data between 5 and 35K. At low temperatures, the direction of minimal susceptibility coincides with the direction of growth of the needle-shaped crystals (approximately along the crystallographic direction \mathbf{a}). With this field orientation, labeled \mathbf{H}_{\parallel} in Fig. 2b, one only observes the magnetic transition at T_{N1} . The transition at T_{N2} is clearly visible in measurements with the field applied *perpendicular* to the \mathbf{a} axis, i.e., in the $\mathbf{b}^* - \mathbf{c}^*$ plane. By rotating the crystal around its needle axis, we have determined the secondary easy magnetic directions in this plane. This is shown in Fig. 2d. The minimum and maximum of the magnetization were found for the crystal rotated $\phi_{min} = -40^\circ$ and $\phi_{max} = 50^\circ$ away from the \mathbf{c}^* direction, respectively. The temperature dependence of the

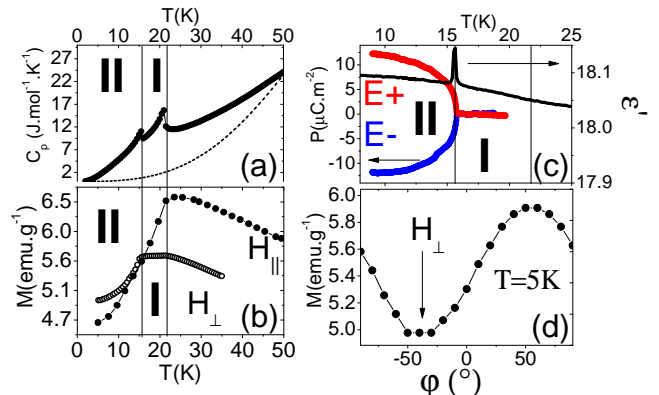


FIG. 2: Magneto-electric phase diagram for FeVO_4 . (a) Heat capacity (filled circles). The dashed line shows the estimated lattice Debye contribution (see text for details) (b) Single crystal magnetization at 3 Tesla with the magnetic field applied in the directions \mathbf{H}_{\parallel} (filled circles) and \mathbf{H}_{\perp} (open circles) explicated in the panel (e). c) Bulk electric polarization measured for a sample cooled in a positive ($E+$, red) and negative ($E-$, blue) electric field of 160V and dielectric constant (black solid line) d) Angular dependence of the magnetization at 3 Tesla and $T=5\text{K}$ measured varying the orientation of the applied magnetic field in the $(\mathbf{b}^*, \mathbf{c}^*)$ plane. \mathbf{H} is aligned with \mathbf{c}^* when $\phi = 0$.

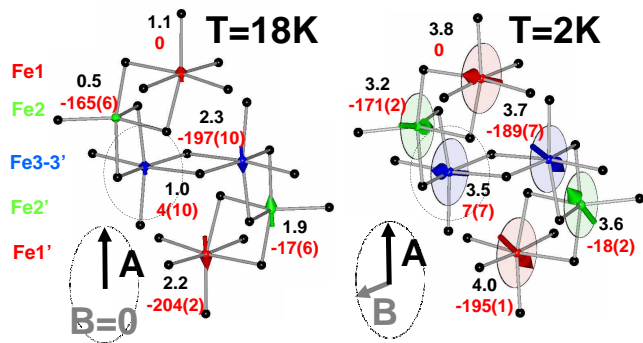


FIG. 3: (Color) Zoom in on the magnetic order of the Fe S -shaped cluster of Fig.4 containing the surrounded spin. The three inequivalent Fe sites are shown as small red, green and blue spheres, and the Fe sites with primed labels are obtained by inversion symmetry. The Fe are arranged in two types of edge-sharing polyhedra: two Fe^{3+}O_5 trigonal bipyramids (sites 2-2') and the 4 other sites in Fe^{3+}O_6 octahedra. Spin are aligned with a common direction \mathbf{A} at $T=18\text{K}$, and rotate in the same (\mathbf{A}, \mathbf{B}) plane at $T=2\text{K}$. The magnetic moment amplitudes (black labels) were calculated using equation 1 with the refined parameters given in the supplementary information[17], accounting for a de-phasing term of 68.4° coming from the position of the cluster in the crystal ($\mathbf{R}_n = (0 \bar{2} 1)$). Only the values of the refined phases φ_j are given in degrees (red labels) for clarity.

magnetization with the field orientation ϕ_{min} , labeled as \mathbf{H}_\perp in Fig. 2b shows a pronounced drop below T_{N2} [16]. The phase boundaries indicated in Fig. 2 therefore mark the domains of stability of two distinct magnetic phases (I and II). The temperature dependence of the dielectric susceptibility, shown in Fig. 2(c), has no anomaly at T_{N1} but the sharp peak at T_{N2} and the concomitant appearance of an electrical polarization (Fig. 2c) demonstrates that the system becomes ferroelectric in phase II, while phase I is not ferroelectric. The value of the electrical polarization at low temperatures is an order of magnitude smaller than for TbMnO_3 [4], a large reduction which can be partly attributed to the fact that our dielectric measurements were made on polycrystalline samples.

The magnetic structures of phases I and II were determined by single-crystal neutron diffraction. Below T_{N1} , the data show new Bragg peaks of magnetic origin, which can all be indexed with a single, nearly temperature-independent propagation vector $\mathbf{k} = (0.222 \ -0.089 \ 0.012)$ almost perpendicular to \mathbf{c} . In the most general case of a single- \mathbf{k} incommensurately modulated structure, the magnetic moments $\mathbf{M}_j(\mathbf{R}_l)$ on a given crystallographic site describe an ellipse as they propagate in different unit cells \mathbf{R}_l . $\mathbf{M}_j(\mathbf{R}_l)$ can therefore be written as:

$$\mathbf{M}_j(\mathbf{R}_l) = \mathbf{A}_j \cos(2\pi \cdot \mathbf{k} \cdot \mathbf{R}_l + \varphi_j) + \mathbf{B}_j \sin(2\pi \cdot \mathbf{k} \cdot \mathbf{R}_l + \varphi_j) \quad (1)$$

where \mathbf{A}_j and \mathbf{B}_j are two perpendicular vectors defining the major and minor semiaxes of the ellipse[18]. An

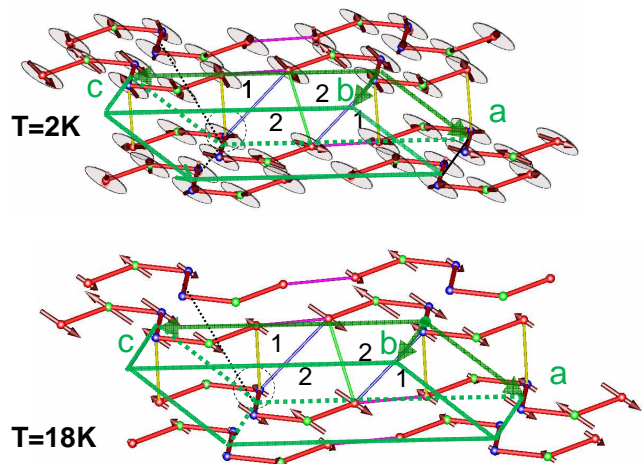


FIG. 4: (Color) Magnetic structure of FeVO_4 as derived from refinements of the single crystal neutron diffraction data $T = 2\text{K}$ (top) and $T = 18\text{K}$ (bottom). The magnetic moments are shown as brown arrows. For the non-collinear structure at 2K , the envelop of the helicoidal modulation is also shown by grey ellipses at each lattice site. Frustrated exchange loops are reproduced from Fig.1, and one spin on loop 1 experiencing the geometrical exchange frustration is surrounded.

initial set of refinements indicated that the magnetic structure of phase I is a *collinear* spin-density wave (i.e., $\mathbf{B}_j = 0$), whereas phase II possesses a *helical* structure. It is noteworthy that the collinear direction of the spins in phase I coincides with the major semiaxis \mathbf{A}_j of the ellipses in phase II, indicating that the spin anisotropy does not change at the phase boundary. In principle, both the amplitudes and directions of \mathbf{A}_j and \mathbf{B}_j as well as the phase angles of the modulations can be different for each site. We have shown that the correlation between parameters can be significantly reduced by introducing constraints [17] whilst still yielding refinements of excellent quality. This has lead us to consider only minimal models for phase I (10 parameters, $R_{F2} = 10.3\%$ and $\chi^2 = 1.7$) and phase II (14 parameters, $R_{F2} = 5.07\%$ and $\chi^2 = 8.2$). The constraints retained suggest that the data do not support significantly different orientations of the ellipses and that the amplitudes $|\mathbf{A}_j|$ and $|\mathbf{B}_j|$ (fig.3) of atoms related by centro-symmetry do not differ significantly, although their phases are not related by centro-symmetry and need to be determined independently. Perspective views of the magnetic structures of phases I and II are shown for one cluster in Fig. 3 and for few clusters in Fig.4.

The helical magnetic order reveals different degree of frustration in different directions. It is characterized by the presence of quasi-1D AF order on chains of S -shaped clusters running in the \mathbf{c} direction. The SSE path linking clusters in this direction is therefore probably the least frustrated SSE interaction inducing only very slow rotations of the average AF direction over a very long period

of approximately 110 nm. This contrasts with all the other SSE pathes, which induce large rotations of the average AF direction between neighboring chains.

Noteworthy, none of the magnetic orders is centrosymmetric because the difference between the phases of sites related by inversion symmetry deviates significantly from 180° and similar phases are refined at $T=2\text{K}$ and $T=18\text{K}$ (Fig.3). This inversion symmetry breaking is clearly visible at $T=2\text{K}$. Each half cluster of 3 Fe shows an almost perfect AF order, but between the two halves, the AF directions are canted by $15 \sim 20^\circ$. The collinear magnetic order at $T=18\text{K}$ simply appears as the projection of the helical order on the common \mathbf{A} direction. We argue that the observed \mathbf{k} vector and the refined phases are here fixed by the symmetric part of the Heisenberg magnetic exchange energy independently of the presence or not of a \mathbf{B} component, and that other energy terms control the stability of the collinear state with respect to the non collinear state.

The transition to collinear magnetic order in multiferroic magnets with a spiral ground state has already been discussed by Mostovoy[10]. At the temperature T_{N2} , there is a cross-over between a high temperature regime in which anisotropy dominates so that the moments align along the local easy axis, and one in which competition between anisotropy and entropy favors disordered components of moment in directions orthogonal to it. For FeVO_4 the local easy axis is the \mathbf{A} direction deduced from the neutron data, which coincides with the macroscopic easy axis, labelled \mathbf{H}_\parallel determined from the magnetisation measurements and labelled \mathbf{H}_\parallel in Fig. 2b. In phase II the moments are confined to the plane of the ellipses with \mathbf{A} and \mathbf{B} as semi-axes, drawn in Figs 3 and 4. When a field is applied in any direction orthogonal to \mathbf{A} (\mathbf{H}_\perp) the temperature dependence of the magnetisation shows a singularity at T_{N2} , a rapid fall below T_{N2} and almost no singularity at T_{N1} . The orthogonal direction for which the fall is most pronounced is parallel to \mathbf{B} , the minor axis of the ellipse. The non-collinearity of phase II is due to the stabilization of the second order parameter modulating moments oriented parallel to \mathbf{B} ; it reflects the presence of additional terms in the free energy which outweigh the entropy effect. The non-collinearity suggests that these terms are due to antisymmetric spin-orbit coupling of the Dzyaloshinski-Morya type proportional to vector products of spins $\mathbf{S}_i \times \mathbf{S}_j$. Most theories of multiferroic spiral magnets have invoked this interaction as the driving force leading to magnetically induced ferro-electricity. However it is not yet clear whether it is spin currents associated with these terms[9], or the simultaneous emergence of ion displacements linked to configurational asymmetry in the magnetic structure,[19] which give the larger contribution to the ferroelectric polarisation.

In summary, we have demonstrated magnetically induced ferroelectricity in FeVO_4 . It is noteworthy that its

magnetoelectric phase diagram in the vicinity of T_{N2} is very similar to that of the classical TbMnO_3 system in the vicinity of $T_{lock}=27\text{K}$ [4, 20]. This gives a strong indication that spin-orbit interactions may make an important contribution to the electrical polarization in FeVO_4 . However, the Fe^{3+} ion has $L=0$ in the free-ion state and in FeVO_4 should be orbitally quenched which reinforces the *induced* nature of the mechanisms responsible for multiferroic behavior in spiral magnets. The magnetoelectric coupling is simpler in FeVO_4 , because the only magnetic atoms participating are Fe; it therefore not influenced or complicated by rare earth magnetism, as this is the case in TbMnO_3 [20].

This study of FeVO_4 has clarified the relative roles of exchange frustration, anisotropy, entropy, and antisymmetric exchange in defining the magnetic state of “type-II” multiferroics. In TbMnO_3 it is difficult to identify the origin of the magnetic frustration because the SSE interactions form a network of next nearest neighbor superexchange interactions. In FeVO_4 on the other we have established a clear connection between the moment reduction or the spin rotations, which are typical of the incommensurate magnetic phases of spiral magnets, and the most relevant SSE paths giving rise to frustration.

We would like to thank Dr J. A. Rodriguez-Velazman for his support during the neutron diffraction experiment.

-
- [1] W. Eerenstein, N. D. Mathur, and J. F. Scott, *Nature* **442**, 759 (2006).
 - [2] S.-W. Cheong and M. Mostovoy, *Nat. Mater* **6**, 13 (2007).
 - [3] N. Rogado, G. Lawes, D. Huse, A. Ramirez, and R. Cava, *Solid State Commun.* **124**, 229 (2002).
 - [4] T. Kimura, T. Goto, H. Shintani, K. Ishizaka, T. Arima, and Y. Tokura, *Nature* **426**, 55 (2003).
 - [5] T. Kimura, Y. Sekio, H. Nakamura, T. Siegrist, and A. P. Ramirez, *Nat. Mater.* **7**, 291 (2008).
 - [6] C. Jia, S. Onoda, N. Nagaosa, and J. H. Han, *Phys. Rev. B* **76**, 144424 (2007).
 - [7] Y. J. Choi, H. T. Yi, S. Lee, Q. Huang, V. Kiryukhin, and S.-W. Cheong, *Phys. Rev. Lett.* **100**, 047601 (2008).
 - [8] L.C. Chapon, P.G. Radaelli, G.R. Blake, S. Park, and S.W. Cheong, *Phys. Rev. Lett.* **96**, 097601 (2006).
 - [9] H. Katsura, N. Nagaosa, and A. V. Balatsky, *Phys. Rev. Lett.* **95**, 057205 (2005).
 - [10] M. Mostovoy, *Phys. Rev. Lett.* **96**, 067601 (2006).
 - [11] M. Fiebig, T. Lottermoser, D. Frohlich, A. Goitsev, and R. Pisarev, *Nature* **419**, 818 (2002).
 - [12] L. M. Levinson and B. M. Wanklyn, *J. Solid State Chem.* **3**, 131 (1971).
 - [13] B. Robertson and E. Kostiner, *J. Solid State Chem.* **4**, 29 (1972).
 - [14] J. Rodriguez-Carvajal, *Physica B* **192**, 55 (1993).
 - [15] This observation is consistent with a strong magnetic diffuse scattering signal above T_{N2} , in neutron powder diffraction experiments, which we also performed separately in the $T_{N1} < T < 30\text{K}$ temperature range. A more

detailed account of all these observations will be reported elsewhere.

- [16] The measurements in all configurations ($\mathbf{H}\perp$ and $\mathbf{H}\parallel$) are in fact both sensitive to T_{N1} and T_{N2} . This is due to the fact the crystal was misaligned with the rotator axis, leading to ~ 10 degrees errors in precision for all the given directions.
- [17] See EPAPS Document No. [number will be inserted by AIP] for the details of the refinement procedure, the parameters, and reliability factors of the neutron diffraction study of the magnetic structures of FeVO_4 . For more information on EPAPS, see <http://www.aip.org/pubservs/epaps.html>.
- [18] O. Zaharko, A. Daoud-Aladine, S. Streule, J. Mesot, P.-J. Brown, and H. Berger, Phys. Rev. Lett. **93**, 217206 (2004).
- [19] H. J. Xiang, S.-H. Wei, M.-H. Whangbo, and J. L. F. DaSilva, Phys. Rev. Lett. **101**, 037209 (2008).
- [20] O. Prokhnenko, R. Feyerherm, M. Mostovoy, N. Aliouane, E. Dudzik, A. U. B. Wolter, A. Maljuk, and D. N. Argyriou, Phys. Rev. Lett. **99**, 177206 (2007).

Supplementary information: Multiferroicity and spiral magnetism in FeVO₄ with quenched Fe orbital moments

(Dated: November 2, 2018)

In the case of FeVO₄, the modulation and the symmetry of magnetic structures is more conveniently described in an alternative cell setting $(\mathbf{a}, \mathbf{b}, \mathbf{c}) = (\mathbf{a}', \mathbf{b}', -2\mathbf{a}' - \mathbf{c}')$, where $(\mathbf{a}', \mathbf{b}', \mathbf{c}')$ was the cell used in the original structural description given in Ref.1. In the original work, cell parameter at RT are $\mathbf{a}' = 6.71633 \text{ \AA}$, $\mathbf{b}' = 8.06817 \text{ \AA}$, $\mathbf{c}' = 9.34715 \text{ \AA}$, $\alpha' = 96.6537^\circ$, $\beta' = 106.528^\circ$, $\gamma' = 101.499^\circ$, so that with our new setting, $\mathbf{a} = 6.71633 \text{ \AA}$, $\mathbf{b} = 8.06817 \text{ \AA}$, $\mathbf{c} = 14.01312 \text{ \AA}$, $\alpha = 74.432^\circ$, $\beta = 140.248^\circ$, $\gamma = 101.499^\circ$. The transformed Fe atomic positions in this new cell are given in table I.

Atom	x	y	z
Fe ₁	-0.06433	0.69426	-0.40839
Fe ₂	0.04169	0.89000	-0.21254
Fe ₃	0.05455	0.69432	0.01143
Fe ₄	-0.05450	0.30573	-0.01143
Fe ₅	-0.04169	0.11000	0.21250
Fe ₆	0.06443	0.30584	0.40839

TABLE I: Atomic positions for FeVO₄ in the transformed cell $(\mathbf{a}, \mathbf{b}, \mathbf{c})$ (see text)

The magnetic moments $\mathbf{M}_j(\mathbf{R}_l)$ of any site j in a unit-cell translated by a vector R_l with respect to the origin is written:

$$\mathbf{M}_j(\mathbf{R}_l) = \mathbf{A}_j \cos(2\pi\mathbf{k} \cdot \mathbf{R}_l + \varphi_j) + \mathbf{B}_j \sin(2\pi\mathbf{k} \cdot \mathbf{R}_l + \varphi_j) \quad (1)$$

where the constraint $(\mathbf{A}_j \perp \mathbf{B}_j)$ is always imposed in our refinements. In FeVO₄, the propagation vector is $\mathbf{k} = (0.222 \text{ } -0.089 \text{ } 0.012)$.

In the program Fullprof[2], we can constrain the direction of the parameters describing the magnetic structure. This is best done using spherical coordinates attached to a (x, y, z) orthogonal frame and defined in a way such as x coincides with \mathbf{a} and z coincides with \mathbf{c}^* .

For amplitude modulated phases ($\mathbf{B}_j=0$) (table II), we use the conventional latitude and azimuth spherical angles (ϕ_j, θ_j) with $(\phi_j, \theta_j) = (0, 0)$ giving z , and $(\phi_j, \theta_j) = (0, 90^\circ)$ giving x , in order to parameterize and/or constrain the \mathbf{A}_j directions .

For helicoidal structures, we used the option in Fullprof which orients the vectors $(\mathbf{A}_j, \mathbf{B}_j)$ and the vector \mathbf{N}_j normal to the $(\mathbf{A}_j, \mathbf{B}_j)$ plane along the axis of orthogonal coordinate systems (x', y', z') obtained by applying active rotations given by the Euler angles $(\phi_j, \theta_j, \chi_j)$, which rotates the (x, y, z) coordinate frame in turn along z , y , and z again. The parameters χ_j are in fact always constrained to be the same for all sites to avoid correlations with the phases φ_j (table III).

[1] B. Robertson and E. Kostiner, J. Solid State Chem. **4**, 29 (1972).

[2] J. Rodriguez-Carvajal, Physica B **192**, 55 (1993).

Model I: fixed directions A				
for all sites and symmetry constraints on phases				
$(R_B = 38.9\% \chi^2 = 32.4 : \text{not converging})$				
Atom	$ \mathbf{A} $	$\phi(^{\circ})$	$\theta(^{\circ})$	$\varphi(^{\circ})$
Fe ₁	3.5(2)	$\phi_1 = 6(3)$	$\theta_1 = 94(3)$	0
Fe ₂	2.9(2)	$\phi_2 = \phi_1$	$\theta_2 = \theta_1$	167(2)
Fe ₃	2.8(2)	$\phi_3 = \phi_1$	$\theta_3 = \theta_1$	-20(3)
Fe ₄	$ A_3 $	$\phi_4 = \phi_1$	$\theta_4 = \theta_1$	$\varphi_3 + 180$
Fe ₅	$ A_2 $	$\phi_5 = \phi_1$	$\theta_5 = \theta_1$	$\varphi_2 + 180$
Fe ₆	$ A_1 $	$\phi_6 = \phi_1$	$\theta_6 = \theta_1$	$\varphi_1 + 180$

Model II: model I +				
partial relaxation of the spin directions				
$(R_B = 39.9\% \chi^2 = 33.7 : \text{not converging})$				
Atom	$ \mathbf{A} $	$\phi(^{\circ})$	$\theta(^{\circ})$	$\varphi(^{\circ})$
Fe ₁	3.5(2)	10(6)	87(7)	0
Fe ₂	2.7(3)	4(7)	98(8)	169(2)
Fe ₃	2.7(2)	5(7)	96(9)	-20(3)
Fe ₄	$ A_3 $	$\phi_4 = \phi_3$	$\theta_4 = \theta_3$	$\varphi_3 + 180$
Fe ₅	$ A_2 $	$\phi_5 = \phi_2$	$\theta_5 = \theta_2$	$\varphi_2 + 180$
Fe ₆	$ A_1 $	$\phi_6 = \phi_1$	$\theta_6 = \theta_1$	$\varphi_1 + 180$

Model III: Model I +				
relaxation of the symmetry constraints on phases				
$(R_B = 10.3\% \chi^2 = 1.64)$				
Atom	$ \mathbf{A} $	$\phi(^{\circ})$	$\theta(^{\circ})$	$\varphi(^{\circ})$
Fe ₁	3.01(5)	$\phi_1 = 3.9(5)$	$\theta_1 = 95.6(6)$	0
Fe ₂	3.23(5)	$\phi_2 = \phi_1$	$\theta_2 = \theta_1$	-165(6)
Fe ₃	2.86(3)	$\phi_3 = \phi_1$	$\theta_3 = \theta_1$	4(10)
Fe ₄	$ A_3 $	$\phi_4 = \phi_1$	$\theta_4 = \theta_1$	-197(10)
Fe ₅	$ A_2 $	$\phi_5 = \phi_1$	$\theta_5 = \theta_1$	-17(6)
Fe ₆	$ A_1 $	$\phi_6 = \phi_1$	$\theta_6 = \theta_1$	-204(2)

Model IV: model I +				
relaxation of the spin directions (partial)				
and phases symmetry constraints				
$(R_B = 10.2\% \chi^2 = 1.62)$				
Atom	$ \mathbf{A} $	$\phi(^{\circ})$	$\theta(^{\circ})$	$\varphi(^{\circ})$
Fe ₁	3.00(5)	3(2)	95(2)	0
Fe ₂	3.23(5)	7(2)	94(2)	-168(9)
Fe ₃	2.88(4)	1(2)	97(2)	3(2)
Fe ₄	$ A_3 $	$\phi_4 = \phi_3$	$\theta_4 = \theta_3$	-197(2)
Fe ₅	$ A_2 $	$\phi_5 = \phi_2$	$\theta_5 = \theta_2$	-20(9)
Fe ₆	$ A_1 $	$\phi_6 = \phi_1$	$\theta_6 = \theta_1$	-203(2)

TABLE II: Magnetic parameters refined at T=18K

Model I: fixed directions for all sites and symmetry constraints on phases ($R_B = 27.9\%$ $\chi^2 = 270.0$: not converging)						
Atom	A	B	$\chi(^{\circ})$	$\phi(^{\circ})$	$\theta(^{\circ})$	$\varphi(^{\circ})$
FE ₁	4.0(5)	4.6(5)	$\chi_1 = -55(5)$	$\phi_1 = 87(6)$	$\theta_1 = 41.3(6)$	0
FE ₂	3.1(5)	3.3(5)	$\chi_2 = \chi_1$	$\phi_2 = \phi_1$	$\theta_2 = \theta_1$	188(3)
FE ₃	5.0(4)	3.3(5)	$\chi_3 = \chi_1$	$\phi_3 = \phi_1$	$\theta_3 = \theta_1$	21(2)
FE ₄	A ₃	B ₃	$\chi_4 = \chi_1$	$\phi_4 = \phi_1$	$\theta_4 = \theta_1$	$\varphi_3 + 180$
FE ₅	A ₂	B ₂	$\chi_5 = \chi_1$	$\phi_5 = \phi_1$	$\theta_5 = \theta_1$	$\varphi_2 + 180$
FE ₆	A ₁	B ₁	$\chi_6 = \chi_1$	$\phi_6 = \phi_1$	$\theta_6 = \theta_1$	$\varphi_1 + 180$
Model II: model I + relaxation of the phases symmetry constraints ($R_B = 5.07\%$ $\chi^2 = 8.24$)						
Atom	A	B	$\chi(^{\circ})$	$\phi(^{\circ})$	$\theta(^{\circ})$	$\varphi(^{\circ})$
FE ₁	4.51(7)	3.67(8)	$\chi_1 = -77(2)$	$\phi_1 = 81(2)$	$\theta_1 = 33.2(1)$	0
FE ₂	4.18(6)	3.16(7)	$\chi_2 = \chi_1$	$\phi_2 = \phi_1$	$\theta_2 = \theta_1$	-171(2)
FE ₃	4.29(7)	3.39(9)	$\chi_3 = \chi_1$	$\phi_3 = \phi_1$	$\theta_3 = \theta_1$	7(7)
FE ₄	A ₃	B ₃	$\chi_4 = \chi_1$	$\phi_4 = \phi_1$	$\theta_4 = \theta_1$	-189(7)
FE ₅	A ₂	B ₂	$\chi_5 = \chi_1$	$\phi_5 = \phi_1$	$\theta_5 = \theta_1$	-18(2)
FE ₆	A ₁	B ₁	$\chi_6 = \chi_1$	$\phi_6 = \phi_1$	$\theta_6 = \theta_1$	-195.2(7)
Model III: Model II + partial relaxation of the directions constraints ($R_B = 6.29\%$ $\chi^2 = 12.7$: slightly diverging)						
Atom	A	B	$\chi(^{\circ})$	$\phi(^{\circ})$	$\theta(^{\circ})$	$\varphi(^{\circ})$
FE ₁	4.52(8)	3.7(1)	$\chi_1 = -76(2)$	76(2)	20.7(5)	0
FE ₂	4.21(8)	3.06(9)	$\chi_2 = \chi_1$	73(2)	28.8(3)	-167(9)
FE ₃	4.31(8)	3.4(2)	$\chi_3 = \chi_1$	85(3)	42.6(3)	0(7)
FE ₄	A ₃	B ₃	$\chi_4 = \chi_1$	$\phi_4 = \phi_3$	$\theta_4 = \theta_3$	-196(7)
FE ₅	A ₂	B ₂	$\chi_5 = \chi_1$	$\phi_5 = \phi_2$	$\theta_5 = \theta_2$	-15(9)
FE ₆	A ₁	B ₁	$\chi_6 = \chi_1$	$\phi_6 = \phi_1$	$\theta_6 = \theta_1$	-196.2(9)

TABLE III: Magnetic parameters refined at T=2K